Low Temperature Physics/Fizika Nizkikh Temperatur, 2012, v. 38, No. 7, pp. 833–841

Antiferromagnet–ferromagnet transition in the cobaltites

I.O. Troyanchuk, M.V. Bushinsky, and D.V. Karpinsky

Scientific-Practical Materials Research Centre of NAS of Belarus
19 P. Brovka Str., Minsk 220072, Belarus

V.A. Sirenko

B. Verkin Institute for Low Temperature Physics and Engineering of the National Academy of Sciences of Ukraine
47 Lenin Ave., Kharkov 61103, Ukraine
E-mail: sirenko@ilt.kharkov.ua

Received March 13, 2012

The three series oxygen-deficient cobaltites $La_{0.5}Ba_{0.5}CoO_{3-\delta}$, $LnBaCo_2O_{5.5}$ and $Sr_2YCo_4O_{10.5}$ have been studied. It has been shown that $La_{0.5}Ba_{0.5}CoO_3$ is an insulating ferromagnet whereas $La_{0.5}Ba_{0.5}CoO_{2.75}$ is a pure antiferromagnet in which the oxygen vacancies are disordered. The oxygen-vacancies ordering leads to appearance of the ferromagnetic component apparently due to a formation of the noncollinear magnetic structure. The antiferromagnet–"ferromagnet" transition is accompanied by a giant magnetoresistance. It is suggested that in the ferromagnetic oxidized compounds Co^{3+} and Co^{4+} ions adopt intermediate spin state whereas for antiferromagnetic (Co^{4+}-free) compositions Co^{3+} ions have high-spin state (pyramids CoO_5) and dominant low-spin state (octahedra CoO_6). In both ferromagnetic and antiferromagnetic compounds the superexchange via oxygen plays an essential role in a formation of the magnetic properties.

PACS: 75.50.Dd Nonmetallic ferromagnetic materials;
75.30.–m Intrinsic properties of magnetically ordered materials;
75.60.Ej Magnetization curves, hysteresis, Barkhausen and related effects.

Keywords: antiferromagnet, oxygen vacancies, spin state transition, layered perovskite.

1. Ferromagnetic and antiferromagnetic phases in the anion deficient cobaltites with disordered oxygen vacancies

Rare earth cobaltites $Ln_{1-x}A_xCoO_3$ (Ln = lanthanide, A = alkaline earth metal: Ca, Sr or Ba) with perovskite structure attract much interest as they exhibit a variety of unusual magnetic and transport properties [1–5]. The Co ions in octahedral symmetry may have either high, intermediate or low-spin state as the energies of the crystalfield splitting of both the Co *3d* states and the Hund's rule exchange energy are comparable. In the ground state at low temperature, $LaCoO_3$ contains Co^{3+} ions with the low-spin electronic configuration $t_{2g}^6e_g^0$ [1–3]. Upon heating, the spin state of Co ions thermally activates to the intermediate state (IS, $t_{2g}^5e_g^1$, $S = 1$) or high-spin state (HS, $t_{2g}^4e_g^2$, $S = 2$) [1–3].

In the hole-doped cobaltites, $La_{1-x}A_xCoO_3$, the additional Co^{4+} ion increases the complexity of the system as it can also be in the different spin states. Among doped cobaltites, the system $La_{1-x}Sr_xCoO_3$ is the most extensively investigated. A spin glass behavior was reported for $x < 0.18$ as well as a ferromagnetic long-range ordering that coincides with concentration insulator-to-metal transition for $x \approx 0.18$ [6]. Similar metallic ferromagnetic state was observed in barium-doped cobaltites with barium content $x > 0.2$ [7–9]. The structural studies performed on the cubic oxygen-stoichiometric perovskite $La_{0.5}Ba_{0.5}CoO_3$ have revealed an onset of a long-range tetragonal phase accompanying a para-ferromagnetic transition at $T_C \approx 180$ K [10,11]. The tetragonal distortion has been discussed in terms of cooperative Jahn–Teller distortions of the CoO_6 octahedra. It was assumed that the Jahn–Teller effect is favored by the intermediate spin-state configuration of the $Co^{3+}(d^6)$ and $Co^{4+}(d^5)$ ions derived from the measured ferromagnetic moment $-1.9\ \mu_B$ per cobalt ion. However, the Sr-doped ferromagnetic cobaltites have approximately the same magnetic moment value and do not exhibit any structural transition at the Curie point [12,13]. Moreover the extended x-ray absorption fine structure (EXAFS) and neutron diffraction studies do not reveal any appreciable local Jahn–Teller distortion in $La_{1-x}Sr_xCoO_3$ [14]. The nature of the ferromagnetic state in cobaltites was a subject of debates for a long time [15–17]. Three main

mechanisms explaining magnetic properties of mixed-valence cobaltites were suggested: the superexchange model based on the localized electron interaction via oxygen ion, the Zener double exchange via charge transfer and the itinerant electron ferromagnetism [15–17].

Besides the alkaline earth doping there is another way to manipulate the physical properties of the rare earth cobaltites. In accordance with [18,19] the oxygen deficiency in $La_{0.5}A_{0.5}CoO_{3-\delta}$ (A = Sr, Ba) perovskites is accompanied by a strong decrease of magnetization and phase separation phenomenon. The crystal structure of the $La_{0.5}Ba_{0.5}CoO_{3-\delta}$ has been analyzed using x-ray, neutron and synchrotron diffraction techniques. The XRD data obtained at room temperature verify the cubic structure of the $La_{0.5}Ba_{0.5}CoO_{3-\delta}$ up to concentration $x = 0.45$. The neutron diffraction data for the $La_{0.5}Ba_{0.5}CoO_{3-\delta}$ sample cooled at a rate of 300 °C/h from 1200 °C have been recorded at temperatures of 300, 150, 80 and 2 K. Rietveld refinement performed for the 300 K NPD pattern assumes cubic symmetry of the compound ($Pm\bar{3}m$ space group). The structural analysis performed by using the tetragonal space group ($P4/mmm$), rhombohedral ($R\bar{3}c$), and orthorhombic one ($Pnma$) did not result in any essential improvement of the reliability factors and cubic structure has been assumed as a more feasible one. The value of the oxygen occupation refined from the NPD data at 300 K is about 2.88, the cubic symmetry supposes a random distribution of the oxygen vacancies as well as of La and Ba ions. The crystal structure has been additionally studied by using synchrotron powder diffraction. In order to estimate the structural parameters in detail, the SPD patterns were recorded in the range from 5 K up to 300 K at the 5 K step. The refinement of the SPD pattern recorded at 300 K, has confirmed the macroscopic cubic symmetry ($Pm\bar{3}m$) of the $La_{0.5}Ba_{0.5}CoO_{2.88}$. However, close inspection of the SPD patterns has revealed a very small asymmetric broadening of the diffraction peaks. The asymmetry becomes more pronounced with temperature decreasing. Similar behavior of the NPD and SPD diffraction peaks excludes possible instrumental faults and/or texturing effects that could lead to an asymmetry of the peaks. Analysis of the NPD and SPD patterns recorded at temperatures below 150 K clarifies a cause of the phase instability. The most probable reason for the peak asymmetry is an appearance of a new phase with structural parameters larger than those for the parent phase. The diffraction patterns recorded at low temperatures have uniquely confirmed the phase separation scenario (Fig. 1). The structure refinement using two-phase model with cubic unit cells for the diffraction patterns obtained for $T < 150$ K, strongly improves the reliability factors. The refined structural data have confirmed gradual extension of the new cubic phase with temperature decrease. The content of the phase with the smaller lattice parameter calculated from the refinement of the NPD pattern recorded at 2 K, is about 70% (the major phase). The

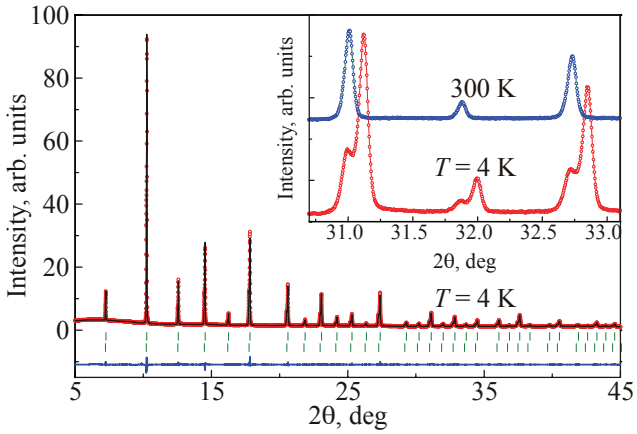

Fig. 1. The synchrotron diffraction spectra for the $La_{0.5}Ba_{0.5}CoO_{3-\delta}$ compound at 4 K. The observed and calculated profiles are noted by points and the line, respectively, the bottom line represents their difference. The data are refined in $Pm\bar{3}m$ space group for the both structural phases. The inset shows the magnified parts of the patterns at 300 K.

rough estimation of the oxygen content performed for the NPD data taken at 2 K, assumes the oxygen content for the phase with the larger lattice parameter to be smaller as compared with the major structural phase. However, the overlapping of the diffraction peaks hampers an accurate determination of the oxygen content for the both structural phases. The difference in the oxygen content assumes a slightly different oxidation state and coordination for Co ions in these phases. One can suggest that in the minor phase Co ions have the oxidation state close to 3+ and are located in the oxygen pyramids and octahedra whereas in the major phase the cobalt ions are placed predominantly in the oxygen octahedra and have a mixed 3+/4+ oxidation state. It should be noted that stoichiometric $La_{0.5}Ba_{0.5}CoO_3$ is a single phase down to the liquid helium temperature [10,11]. So, the oxygen deficit is the important factor in the phase separation.

The NPD data permit to clarify the magnetic structure of the $La_{0.5}Ba_{0.5}CoO_{2.88}$. Taking into account the SPD data for $La_{0.5}Ba_{0.5}CoO_{2.88}$ the additional peaks occurring only on NPD patterns below 150 K can be referred to magnetic neutron scattering. The NPD patterns were well fitted assuming the coexistence of ferromagnetic and *G*-type antiferromagnetic structures. An additional contribution to the intensities of the diffraction peaks (100), (110), (210) testifies long range ferromagnetism within the compound, whereas the new magnetic peaks indexed as (111), (113), (313) in $2a_p \times 2a_p \times 2a_p$ cubic metric assume antiferromagnetic ordering. Based on the structural data the ferromagnetic contribution is attributed to the major structural phase, whereas *G*-type antiferromagnetic one is associated with the minor phase with larger unit cell. The estimated magnetic moments are approximately ~1.6 μ_B for *F*-type phase and ~2 μ_B for *G*-type antiferromagnetic phase. The

calculated moment for the ferromagnetic phase correlates with the published data for the oxygen stoichiometric La and Ba ordered $LaBaCo_2O_6$ (1.5 μ_B) and disordered $La_{0.5}Ba_{0.5}CoO_3$ (1.9 μ_B) ferromagnetic phases [10,11].

The $La_{0.5}Ba_{0.5}CoO_{2.77}$ sample reveal exceptional behavior of the unit cell parameter with temperature change. The unit cell parameter decreases with temperature reduction from room temperature down to ~170 K where pure antiferromagnetic order develops. Whereas below the temperature of antiferromagnetic ordering an unexpected gradual increase of the lattice parameter is observed. The unit cell volume estimated for the $La_{0.5}Ba_{0.5}CoO_{2.77}$ compound at 2 K is close to that observed at room temperature. The phase separation phenomena as well as ferromagnetic contribution into NPD pattern have not been observed.

We suggest that the most probable reason of the unusual expansion of the unit cell as well as phase separation is transition of the Co^{3+} ions to the high/low-spin state from initially an intermediate spin state which is more stable at high temperature. The structural phase separation can be accompanied by redistribution of the electronic density (electronic phase separation). The magnetization data seem to be in agreement with this assumption. The oxidized $La_{0.5}Ba_{0.5}CoO_{3-\delta}$ being cooled slowly from 1200 °C shows magnetic moment about 1.8 μ_B corresponding to the intermediate spin state of the Co^{3+}/Co^{4+} ions for pure ferromagnetic state. Decreasing of the oxygen content lead to drop of the magnetic moment and anomalous magnetization behavior thus indicating the spin-state transition (Fig. 2). The pure antiferromagnetic compositions do not show remnant magnetization. In accordance with [20] we suggest that high-spin state is stabilized in pyramids whereas low-spin state corresponds to octahedra.

A relatively large negative magnetoresistance is observed in nearly stoichiometric oxidized $La_{0.5}Ba_{0.5}CoO_{3-\delta}$. Figure 3 shows the temperature variations of electrical resistivity measured at different external magnetic fields for $La_{0.5}Sr_{0.5}CoO_{3-\delta}$ (upper panel) and $La_{0.5}Ba_{0.5}CoO_{3-\delta}$ (lower panel). Both the samples are pure ferromagnets. The resistivity of $La_{0.5}Sr_{0.5}CoO_{3-\delta}$ exhibits the metallic behavior within the whole measured temperature range from 5 to 300 K. The nonpronounced anomaly in the $\rho(T)$ dependence was observed near the Curie point at the absence of the external magnetic field. The magnetoresistance is not revealed at low temperatures but appeared around T_C, as is shown in Fig. 3. The temperature variation of resistivity for $La_{0.5}Ba_{0.5}CoO_{3-\delta}$ is dramatically different. The metallic behavior of the resistivity has been observed only in the narrow temperature range near the Curie point $T_C \sim 170$ K, and it gradually changes to a semiconducting one below 150 K. An external magnetic field strongly extends the metallic-like temperature range above the Curie point, however at low temperatures the semiconductive behavior does not essentially change. Figure 4 shows magnetoresistance as a function of a field at various temperatures for $La_{0.5}Ba_{0.5}CoO_{3-\delta}$. The magnetoresistance exhibits a local maximum near the T_C and increases gradually with further cooling. At 5 K we obtained the MR value of about 20% in the field of 14 T. The MR varies gradually with the field and does not show any tendency to saturation with the temperature decrease.

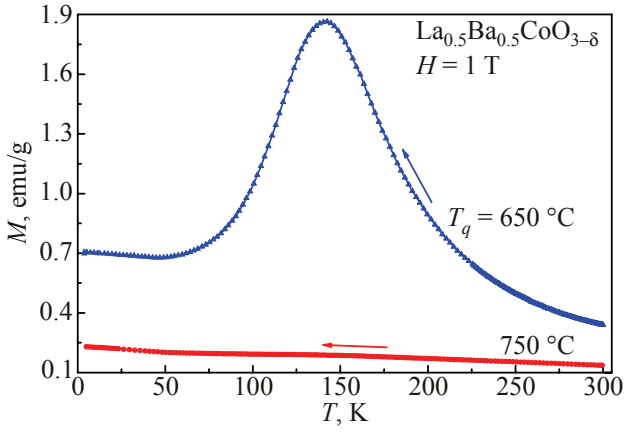

Fig. 2. The magnetization vs temperature dependencies of the $La_{0.5}Ba_{0.5}CoO_{3-\delta}$ quenched from 750 and 650 °C. The arrows indicate temperature change direction.

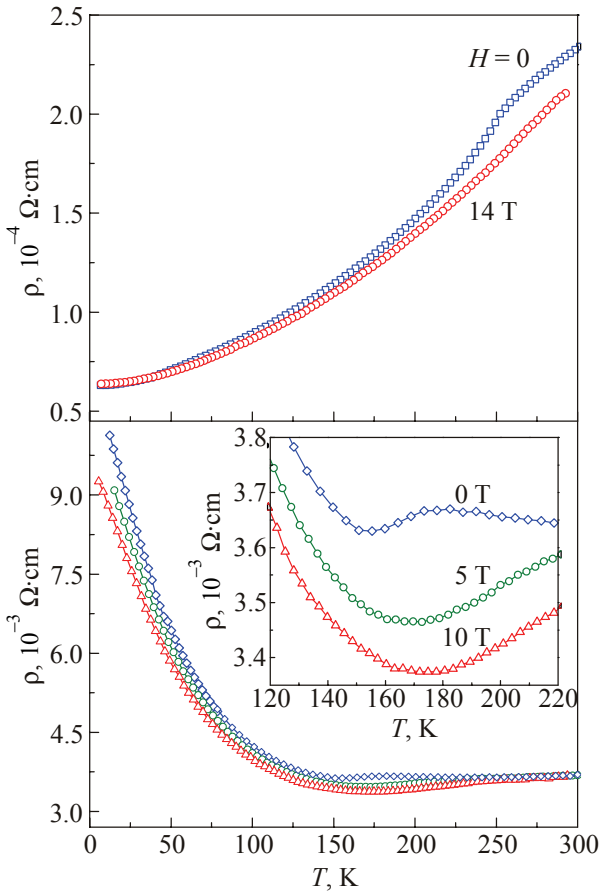

Fig. 3. The resistivity of ferromagnetic $La_{0.5}Sr_{0.5}CoO_{3-\delta}$ (top panel) and $La_{0.5}Ba_{0.5}CoO_{3-\delta}$ (bottom panel) cooled at a rate of 100 °C/h vs temperature. The inset shows the resistivity behavior near the Curie point.

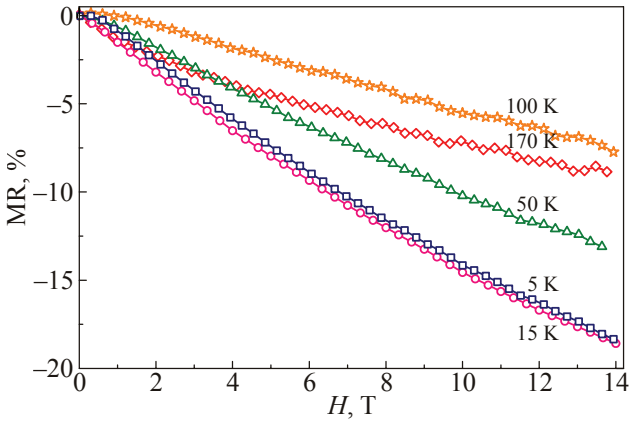

Fig. 4. Field dependencies of the magnetoresistance ratio MR = [ρ(*H*) – ρ(*H* = 0)]/ρ(*H* = 0)·100% for the ferromagnetic $La_{0.5}Ba_{0.5}CoO_{3-\delta}$.

There are different types of the large magnetoresistance ratio observed in the ordinary cobaltites. The large magnetoresistance was observed in the insulating spin-glass phase of the lightly doped $La_{1-x}Sr_xCoO_3$ cobaltites [21,22]. It is suggested that the interface effects associated with different magnetic and conductive states of ferromagnetic clusters and paramagnetic matrix are responsible for nonsaturated magnetoresistance observed in the large magnetic field [21]. This type of magnetoresistance is the most pronounced at low temperature. The second type of large magnetoresistance was observed at the low temperature in the insulating homogeneous ferromagnet $La_{0.5}Ba_{0.5}CoO_3$ [10,11]. This type of magnetoresistance has similar temperature and field dependences with magnetotransport parameters of the lightly doped cobaltites. The magnetoresistance is not saturated in the large magnetic field and strongly increases while temperature decreasing. In contrast to manganites there is no large magnetotransport anomaly in the vicinity of the Curie point. The observation of the homogeneous ferromagnetism in insulating $La_{0.5}Ba_{0.5}CoO_3$ in our opinion, confirms the hypothesis that ferromagnetic properties of the hole-doped cobaltites with the perovskite structure are governed by the superexchange interactions similar to those in oxides of the nonmixed valence type of magnetoactive ions (e.g., ferrites with Fe^{3+} ions). The small magnetotransport and conductivity anomalies near the Curie point of the both insulating and conductive cobaltites apparently do not support the dominant role of the "double exchange" in defining of the ferromagnetic ordering as it was suggested in a number of works [6,10,11]. The insulating character of the $La_{0.5}Ba_{0.5}CoO_3$ ferromagnetic phase cannot be understood by means of the "itinerant magnetism" model. Apparently large magnetoresistance observed in homogeneous $La_{0.5}Ba_{0.5}CoO_3$ at low temperature is associated with decreasing of the insulating gap between e_g and collective t_{2g} state upon external magnetic field.

2. Antiferromagnet–ferromagnet transition in iron doped $TbBaCo_2O_{5.5}$ layered perovskite

The layered perovskites $LnBaCo_2O_{5.5}$ (Ln = lanthanide) have attracted a great attention due to interplay between magnetic and magnetotransport properties [23–26]. The crystal structure of these compounds has an alternating linkage of Ba^{2+} and Ln^{3+} layers along the *c* axis and layers of CoO_5 pyramids and CoO_6 octahedrons along the *a* or *b* axis [25]. As a result of ordering of Ln^{3+} and Ba^{2+} ions as well of oxygen vacancies the crystal structure is described with unit cell $a_p \times 2a_p \times 2a_p$ in the space group *Pmmm*.

The $LnBaCo_2O_{5.5}$ compounds exhibit following transitions: antiferromagnet–"ferromagnet" in the temperature range 200 K ≤ *T* < 260 K, "ferromagnet"–paramagnet (250 K < *T* < 300 K) and metal–insulator (300 K < *T* < 370 K) depending on Ln ion size [23–25]. According to the neutron diffraction studies the "ferromagnetic" phase consists of the basic *G*-type antiferromagnetic ($2a_p \times 2a_p \times 2a_p$) and small ferromagnetic components, while the low-temperature pure antiferromagnetic phase has magnetic unit cell of $2a_p \times 2a_p \times 4a_p$-type [27–30]. The transition antiferromagnet–"ferromagnet" leads to a drop of the resistivity and a giant magnetoresistance effect [23–26]. The reason for interplay between magnetic and magnetotransport properties is not clear so far. In order to understand magnetotransport properties the detailed description of the magnetic structure in the both phases is necessary. Several studies of magnetic structure of the $LnBaCo_2O_{5.5}$ compounds have been performed with diverging results [27–34]. According to [30,34] the magnetic structure is noncollinear in both antiferromagnetic and ferromagnetic phases. The Co^{3+} ions in octahedrons adopt the low-spin state [30,34], whereas in pyramids they are in the high-spin state. In works [27,28] it was suggested that the correct space group is *Pmma* and the crystal structure is described with a $2a_p \times 2a_p \times 2a_p$ supercell. In this model Co^{3+} ions in both pyramidal and octahedral sublattices are located in nonequivalent two sites and magnetic structure can be described by a collinear model for both "ferromagnetic" and antiferromagnetic phases. It worth to be noted that symmetry analysis performed for both space groups *Pmmm* and *Pmma* does not allow realization of the noncollinear magnetic structure with ferromagnetic component. However, a synchrotron x-ray powder diffraction study of $YBaCo_2O_{5.5}$ compound has revealed some additional peaks associated with a $2a_p \times 2a_p \times 2a_p$ crystal structure supercell and small monoclinic distortion in the ferromagnetic phase corresponding space group *P*112/*a* [35]. The observed monoclinic distortion support the model of the noncollinear magnetic structure for description of magnetic and magnetotransport properties of $LnBaCo_2O_{5.5}$-type compounds.

Very intricate properties have been revealed in $TbBaCo_2O_{5.5-x/2}$ doped with Fe^{3+} ions [26,36]. In

$TbBaCo_{2-x}Fe_xO_{5.5}$ below $x = 0.1$ orthorhombic distortion slightly increases with increasing Fe^{3+} content and disappears above $x = 0.15$. The temperature of "ferromagnet"–paramagnet transition increases while the temperature of "ferromagnet"–antiferromagnet transition decreases with increasing Fe^{3+} content up to $x = 0.1$. Transition into tetragonal phase ($x > 0.15$) leads to a collapse of the ferromagnetic phase. The jump of conductivity as well as thermal hysteresis associated with "ferromagnet"–antiferromagnet transition become much larger with Fe doping within orthorhombic phase. The antiferromagnetic phase becomes proof against external magnetic field. Mössbauer study has revealed that Fe^{3+} ions predominantly occupy two strongly distorted positions [36]. The results of measurements of ZFC and FC magnetization of $TbBaCo_{1.9}Fe_{0.1}O_{5.5}$ used for neutron diffraction are shown in Fig. 5. Both ZFC and FC magnetizations exhibit a sharp maxima at $T = 300$ K which indicate the transition into a paramagnetic state. In the temperature interval 200–170 K the field cooled magnetization decreases strongly with lowering temperature. In this temperature range ZFC magnetization changes very little thus indicating a huge magnetic anisotropy. It should be noted that ZFC and FC magnetizations do not coincide below 170 K down to liquid helium temperature due to a presence of a small remnant magnetization. The good agreement between calculated and observed profiles of NPD patterns was reached using *Pmmm* space group with a $2a_p \times a_p \times 2a_p$ unit cell. The refinement in *Pmma* space group with $2a_p \times 2a_p \times 2a_p$ unit cell leads to the same factors of reliability as refinement in terms of *Pmmm* model.

Analysis of the powder patterns collected at the temperature 215 K shows that there is a set of the additional magnetic reflections which could be indexed using a $2a_p \times 2a_p \times 2a_p$ magnetic unit cell. Furthermore the additional contribution into (100) reflection has been clearly observed. This contribution disappears at 130 K. The contribution into reflection (100) corresponds to the ferromagnetic component whereas the appearance of (111), (311), (113), (331) and (313) reflections corresponds to the *G*-type antiferromagnetic component. The contribution into the *G*-type antiferromagnetic component increases with decreasing temperature down to 130 K whereas the ferromagnetic contribution disappears. Such a type of behavior of the antiferromagnetic component was observed first for the $LnBaCo_2O_{5.5}$-type layered perovskites exhibiting antiferromagnet–"ferromagnet" transition. The low-temperature antiferromagnetic phase of the undoped compounds is described with a more complex $2a_p \times 2a_p \times 4a_p$ magnetic unit cell [27–32]. The refinement of the magnetic structure at 215 K gives following values of magnetic moments for the *G*-type antiferromagnetic component: 1.9 μ_B per Co ion for the pyramidal sublattice and 0.9 μ_B for the octahedral one. The ferromagnetic component is 1.0 μ_B per formula unit and directed along the *b* axis, whereas the antiferromagnetic component is along the *a* axis. All the magnetic moments are placed within (*a,b*) plane. Decreasing temperature down to 130 K leads to increasing magnetic moment up to 2.6 μ_B for the pyramidal sublattice while for octahedral one it practically does not change.

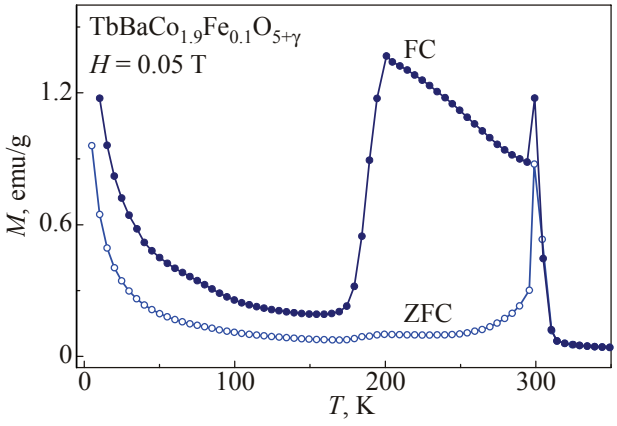

Fig. 5. The temperature dependences of the magnetization for $TbBaCo_{1.9}Fe_{0.1}O_{5+\gamma}$ measured in the FC and ZFC modes at $H = 0.05$ T.

The magnetic moment value in the pyramidal sublattice is 2.6 μ_B per ion at 130 K. This value is significantly more than 2 μ_B associated with the intermediate spin state. It was found that magnetic moments of the high-spin Co^{3+} ions in $Sr_2Co_2O_5$ and $BiCoO_3$ are 3.3 and 3.4 μ_B, respectively [37,38]. However, the magnetic moment of the Co^{3+} ion in high-spin state ($S = 2$) should be about 4 μ_B. So, present data can hardly be adjusted with a pure ionic model for Co ions magnetic moments. In Refs. 2, 3 the Co^{3+} ions in $LaCoO_3$ have been shown to have first excited state corresponding to the high-spin one. Probably it is valid for $LnBaCo_2O_{5.5}$-type compounds. Hence, the description of the magnetic state of Co^{3+} ions in $TbBaCo_2O_{5.5}$ doped with iron could be done in terms of a mixed low/high-spin magnetic state. The results of NMR study of $EuBaCo_2O_{5.5}$ are in agreement with a mixed low-high spin state model [39].

Both "ferromagnetic" and antiferromagnetic phases in $TbBaCo_{1.9}Fe_{0.1}O_{5.5}$ have the *G*-type magnetic structure with a $2a_p \times 2a_p \times 2a_p$ magnetic unit cell. In this magnetic structure there are only two different magnetic positions for both CoO_5 and CoO_6 layers. The transition into the antiferromagnetic phase leads to a substantial increase of magnetic moments in pyramidal sublattice, whereas magnetic moments in the octahedrons remain practically the same. These results can be easily understood in noncollinear model of the magnetic structure of the "ferromagnetic" phase.

Apparently in the ferromagnetic phase an angle between magnetic moments of the Co^{3+} ions in pyramidal sublattice in direction of the *a* axis is about 30°. In the antiferromagnetic phase the magnetic structure seems to be collinear and aligned along the *b* axis because the $2a_p \times 2a_p \times 2a_p$ magnetic unit cell is preserved. Remind, that in the undoped $TbBaCo_2O_{5.5}$ the low-temperature antifer-

romagnetic phase remains noncollinear and the magnetic unit cell contains four sites for magnetic ions which leads to $2a_p \times 2a_p \times 4a_p$ magnetic supercell [34].

In order to understand an origin of noncollinear magnetic structure it is necessary to consider exchange interactions in the pyramidal sublattice. One can suppose exchange interactions in the pyramidal sublattice to be negative in the case when nearest pyramids have common oxygen ion and positive if not. In this case all the interactions within (*a,b)* plane are negative whereas along *c* axis negative and positive ones are alternated. This leads to a frustration of magnetic interactions and the noncollinear magnetic structure in the some temperature range could be more favorable than the simple collinear one. The spin-orbital interaction seems to be also very important factor leading to canting of the magnetic moments. Really the measurements of magnetic and magnetotransport properties performed on a single crystal have revealed a huge magnetocrystalline anisotropy as well as giant anisotropic magnetoresistance [31]. A number of noncollinear magnetic structures in different magnetic materials have been understood in terms of itinerant magnetism approach with relativistic interactions [40]. Doping with Fe^{3+} stabilizes the collinear antiferromagnetic structure at low temperatures because all the interactions Fe^{3+}–Fe^{3+}, Fe^{3+}–Co^{2+}, Fe^{3+}–Co^{3+} seem to be strongly antiferromagnetic. At high Fe doping ($x > 0.1$) the orthorhombic symmetry transforms to tetragonal one leading to ferromagnetic component disappearing [26,36]. The ferromagnetic component collapse is caused by random distribution of the octahedra and pyramids in tetragonal phase.

In the works [27,28] the noncollinear solution has been overruled on the base of symmetry analysis. However the noncollinear magnetic structures in $LnBaCo_2O_{5.5}$ compounds seem to be a result of a very small monoclinic distortion whereas for symmetry analysis only orthorhombic space groups were used. The noncollinear structure is subtle balance between positive, negative exchange interactions and magnetocrystalline anisotropy.

Using the conception of noncollinear magnetism one can try to explain the peculiarities of magnetic and transport properties of the layered cobaltites, associated with "ferromagnet"–antiferromagnet transition. In contrast to collinear model the noncollinear one provides pure ferromagnetic direction orthogonal to antiferromagnetic axis. Hence the transition into noncollinear ferromagnetic phase can produce strong changes in the vicinity of Fermi level. Really in the noncollinear model antiferromagnetic component is aligned along the *a* axis whereas along the *b* axis the *pure* ferromagnetic component is realized thus leading to a jump of conductivity at antiferromagnet–"ferromagnet" transition.

3. Antiferromagnet–ferromagnet transition in layered $Sr_3YCo_4O1_{0.5+\delta}$-type cobaltites

Another class of anion-deficient layered cobaltites was received quite recently. It has the chemical composition $Sr_3LnCo_4O_{10.5+\delta}$ (its reduced chemical formula is $Sr_{0.75}Ln_{0.25}CoO_{3-\gamma}$), where the rare earth ions can partially substitute for strontium ions and vice versa [41–44]. Its crystal structure is built by alternating anion-deficient $CoO_{4+\delta}$ layers and layers formed by CoO_6 octahedra with sharing vertices. This class of compounds is characterized by high magnetic ordering temperature (up to 360 K) [45–47]. Spontaneous magnetization appears below 360 K, attains its maximum value near room temperature, and then decreases gradually down to liquid helium temperatures [45–49]. Several conjectures explaining the anomalous temperature dependence of the magnetization have been put forward. In Ref. 50, it was suggested that a certain fraction of Co^{3+} ions undergo the transition from the high-spin to low-spin state with a decrease in temperature. However, the neutron diffraction studies do not reveal any anomalous decrease in the magnetic moment when the temperature is decreased [48,49,51]. In the whole temperature range below the magnetic ordering point, the antiferromagnetic *G*-type structure was observed, whereas it was impossible to reliably detect the ferromagnetic contribution since it turned out to be quite small. For this reason, in [48,49], the anomalous behavior of the magnetization was attributed to the phase transition from the magnetic state with the spontaneous magnetization to the purely antiferromagnetic state. It was assumed that the transition was incomplete owing to the chemical inhomogeneity of the samples. However, another interpretation of the transition was proposed in Ref. 52, where the ferromagnetic component was determined by the neutron diffraction method. The model proposed in Ref. 52 attributes the anomalous behavior of the magnetization to the presence of a weak magnetic sublattice within the magnetic structure of the collinear ferrimagnet. In the framework of this model, the spontaneous magnetization results from the ordering of cobalt ions with different oxygen coordination numbers in the $CoO_{4+\delta}$ layer, whereas the CoO_6 layer is purely antiferromagnetic. According to Ref. 52, the spontaneous magnetization appears owing to the different temperature dependences of the magnetic moments of cobalt in different sublattices of the collinear ferrimagnet.

The temperature dependence of the magnetization for the $Sr_3YCo_4O_{10.6+\delta}$ sample obtained by fast cooling is shown in Fig. 6. The measurements were performed upon cooling and heating at different magnetic fields up to 14 T. The cooling and heating rates were 0.5 K/min. Within the temperature range of 210–240 K, a steep increase (decrease) in the magnetization with a temperature hysteresis of 12 K has been observed. Such a temperature behavior of the magnetization is characteristic of the first-order mag-

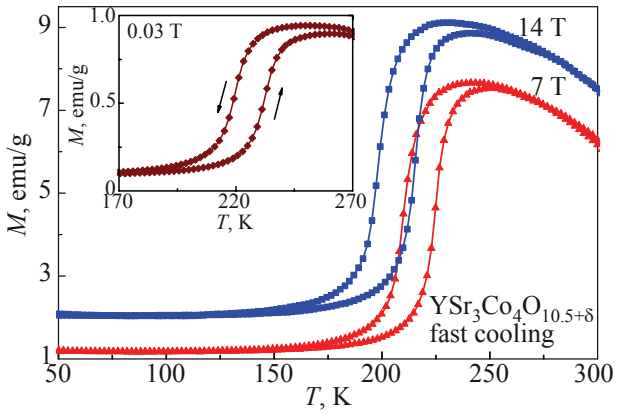

Fig. 6. Temperature dependence of the magnetization for $Sr_3YCo_4O_{10.5+\delta}$ samples produced upon fast cooling from 1000 °C in different magnetic fields.

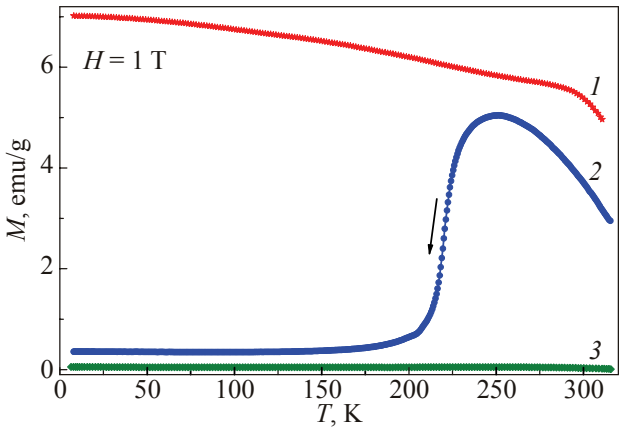

Fig. 7. Temperature dependences of the magnetization for $Sr_{3.2}Y_{0.8}Co_4O_{10.5+\delta}$ (*1*), $Sr_3YCo_4O_{10.5+\delta}$ (*2*), and $Sr_{2.6}Y_{1.4}Co_4O_{10.5+\delta}$ (*3*) samples (H = 1 T).

netic phase transition of the order–order type. In the high-temperature phase, the magnetization is not saturated at magnetic fields up to 14 T. Therefore, it is impossible to determine accurately the spontaneous magnetization. Nevertheless, its estimated value is no less than 0.25 μ_B per cobalt ion. In the temperature range corresponding to the magnetic phase transition, the magnetic field dependence of the magnetization exhibits an anomalous growth of the susceptibility at high fields and a pronounced field hysteresis of the magnetization. Such a behavior of the magnetization is characteristic of metamagnets, i.e., materials where the applied magnetic field induces another phase state with a higher magnetization. The metamagnetic transition is incomplete since a field of 14 T is insufficient to induce a homogeneous high-temperature magnetic phase. At low temperatures (T < 150 K), the magnetic field dependence of the magnetization is almost linear, similar to that in antiferromagnets, whereas the spontaneous magnetization is practically absent. Both slightly reduced and oxidized samples show antiferromagnet–"ferromagnet" transition also.

The new results of the magnetic measurements suggest that the behavior of the magnetization for the $Sr_3YCo_4O_{10.5+\delta}$ sample reported in Refs. 45–49 is associated with inhomogeneous yttrium distribution over the sample. With an increase in the yttrium content, a purely ferromagnetic behavior transforms to a purely antiferromagnetic behavior, passing through intermediate compositions, which exhibit the first-order antiferromagnet–"ferromagnet" phase transition (Fig. 7).

It worth to be noted that the behaviors of two different classes of layered cobaltites, $SrLnCo_4O_{10.5}$ and $LnBaCo_2O_{5.5}$, are very similar. Both classes of layered cobaltites exhibit the antiferromagnet–ferromagnet transition and accurately prepared polycrystalline samples have nearly the same spontaneous magnetization in the ferromagnetic phase. This is likely due to similar mechanisms of ferromagnetism in both classes of compounds, where the antiferromagnet–ferromagnet transition can occur in the nominally *G*-type magnetic structure without the formation of additional magnetic reflections in the low-temperature antiferromagnetic phase [48,49,52,53]. This behavior can be easily explained under the assumption that the magnetic structure of the ferromagnetic phase is noncollinear with the uncompensated magnetic moment as in weak ferromagnets. The symmetry analysis forbidding the existence of noncollinear ferromagnetism in $LnBaCo_2O_{5.5}$ was performed within the framework of the orthorhombic *Pmma* space group [27]. At the same time, a careful x-ray structural analysis indicates that the true symmetry is monoclinic (*P*112/*a*) [35]. It is necessary to note that the true symmetry of $Sr_3YCo_4O_{10.5+\delta}$ is also monoclinic (possible space group *A2/a*) [45] rather than orthorhombic, while the symmetry analysis in Ref. 52 was performed on the basis of the latter symmetry.

4. Conclusions

The insulating $La_{0.5}Ba_{0.5}CoO_3$ and metallic $Ln_{0.5}Sr_{0.5}CoO_3$ ordinary cobaltites are ferromagnetic due to superexchange interactions via oxygen between cobalt ions in the intermediate spin state. The insulating $La_{0.5}Ba_{0.5}CoO_3$ is only one known cobaltite exhibiting cooperative static Jahn–Teller distortions of the CoO_6 octahedra at low temperature. The oxygen content decreasing leads to transformation from ferromagnetic to the *G*-type antiferromagnetic structure through the phase separated state. The anomalous structural and magnetization behavior apparently is associated with a spin state transition. The antiferromagnetic phase is characterized by high/low-spin state of the Co^{3+} ions and lack of the ferromagnetic contribution.

The ordering of the oxygen vacancies in the $LnBaCo_2O_{5.5}$ and $Sr_3YCo_4O_{10.5}$ layered cobaltites lead to increases of the Neel point from 170 to 380 K and appearance of the relatively small ferromagnetic component which is identical for both type of the layered cobaltites.

The ferromagnetic component is associated with noncollinear magnetic structure. The noncollinear structure is subtle balance between positive and negative exchange interactions, magnetocrystalline anisotropy and accompany by lowering of the crystal structure symmetry to satisfy the symmetry criteria. The resistivity drop accompanying antiferromagnet–ferromagnet transition in the $LnBaCo_2O_{5.5}$ seems to be result of a partial collapse of the insulating gap in direction of the pure ferromagnetic component.

The authors would like to acknowledge the financial support of the BRFFI (Grant Nos. T11D-003).

1. J.B. Goodenough and J.S. Zhou, *Structure and Bonding*, Springer, New York (2001).
2. A. Podlesnyak, S. Streule, J. Mesot, M. Medarde, E. Pomjakushina, K. Conder, A. Tanaka, M.W. Haverkort, and D.I. Khomskii, *Phys. Rev. Lett.* **97**, 247208 (2006).
3. M.W. Haverkort, Z. Hu, J.C. Cezar, T. Burnus, H. Hartmann, M. Reuther, C. Zobel, T. Lorenz, A. Tanaka, N.B. Brookes, H.H. Hsieh, H.J. Lin, C.T. Chen, and L.H. Tjeng, *Phys. Rev. Lett.* **97**, 176405 (2006).
4. D.P. Kozlenko, N.O. Golosova, Z. Jirak, L.S. Dubrovinsky, B.N. Savenko, M.G. Tucker, Y. LeGodec, and V.P. Glazkov, *Phys. Rev.* **B75**, 064422 (2007).
5. R.F. Klie, J.C. Zheng, Y. Zhu, M. Varela, J. Wu, and C. Leighton, *Phys. Rev. Lett.* **99**, 047203 (2007).
6. J. Wu and C. Leighton, *Phys. Rev.* **B67**, 174408 (2003).
7. P. Mandal, P. Choudhury, S.K. Biswas, and B. Ghosh, *Phys. Rev.* **B70**, 104407 (2004).
8. M. Kriener, C. Zobel, A. Reichl, J. Baier, M. Cwik, K. Berggold, H. Kierspel, O. Zabara, A. Freimuth, and T. Lorenz, *Phys. Rev.* **B69**, 094417 (2004).
9. A.P. Sazonov, I.O. Troyanchuk, H. Gamari-Seale, V.V. Sikolenko, K.L. Stefanopoulos, G.K. Nikolaides, and Y.K. Atanassova, *J. Phys.: Condens. Matter* **21**, 156004 (2009).
10. F. Fauth, E. Suard, and V. Caignaert, *Phys. Rev.* **B65**, 060401(R) (2001).
11. T. Nakajima, M. Ichihara, and Y. Ueda, *J. Phys. Soc. Jpn.* **75**, 1572 (2005).
12. V. Sikolenko, A. Sazonov, I. Troyanchuk, D. Többens, U. Zimmermann, E. Pomjakushina, and H. Szymczak, *J. Phys.: Condens. Matter* **16**, 7317 (2004).
13. V. Sikolenko, V. Efimov, E. Efimova, A. Sazonov, C. Ritter, A. Kuzmin, and I. Troyanchuk, *J. Phys.: Condens. Matter* **21**, 436002 (2009).
14. N. Sundaram, Y. Jiang, I.E. Anderson, D.P. Belanger, C.H. Booth, F. Bridges, J.F. Mitchell, T. Proffen, and H. Zheng, *Phys. Rev. Lett.* **102**, 026401 (2009).
15. J.B. Goodenough, *Mater. Res. Bull.* **6**, 967 (1971).
16. M. Senaris-Rodriguez and J. Goodenough, *J. Solid State Chem.* **118**, 323 (1995).
17. D. Louca, J.L. Sarrao, J.D. Thompson, H. Roder, and G.H. Kwei, *Phys. Rev.* **B60**, 10378 (1999).
18. I.O. Troyanchuk, D.V. Karpinsky, M.V. Bushinsky, V. Sikolenko, V. Efimov, and A. Cervellino, *JETP Lett.* **93**, 139 (2011).
19. R.P. Haggerty and R. Seshadri, *J. Phys.: Condens. Matter* **16**, 6477 (2004).
20. M. Soda, Y. Yasui, M. Ito, S. Iikubo, M. Sato, and K. Kakurai, *J. Phys. Soc. Jpn.* **73**, 464 (2004).
21. J. Wu, J.W. Lynn, C.J. Glinka, J. Burley, H. Zheng, J.F. Mitchell, and C. Leighton, *Phys. Rev. Lett.* **94**, 037201 (2005).
22. M. Sánchez-Andújar, J. Mira, J. Rivas, and M.A. Señarís-Rodríguez, *Progress in Solid State Chemistry* **35**, 407 (2007).
23. C. Martin, A. Maignan, D. Pelloquin, N. Nguyen, and B. Raveau, *Appl. Phys. Lett.* **71**, 1421 (1997).
24. I.O. Troyanchuk, N.V. Kasper, D.D. Khalyavin, H. Szymczak, R. Szymczak, and M. Baran, *Phys. Rev. Lett.* **80**, 3380 (1998).
25. A. Maignan, C. Martin, D. Pelloquin, N. Nguyen, and B. Raveau, *J. Solid State Chem.* **142**, 247 (1999).
26. I.O. Troyanchuk, A.N. Chobot, D.D. Khalyavin, R. Szymczak, and H. Szymczak, *J. Exp. Theor. Phys.* **95**, 748 (2002).
27. V.P. Plakhty, Yu.P. Chernenkov, S.N. Barilo, A. Podlesnyak, E. Pomjakushina, E.V. Moskvin, and S.V. Gavrilov, *Phys. Rev.* **B71**, 214407 (2005).
28. D.D. Khalyavin, D.N. Argyriou, U. Amann, A.A. Yaremchenko, and V.V. Kharton, *Phys. Rev.* **B75**, 134407 (2007).
29. F. Fauth, E. Suard, V. Caignaert, and I. Mirebeau, *Phys. Rev.* **B66**, 184421 (2002).
30. M. Soda, Y. Yasui, T. Fujita, T. Miyashita, M. Sato, and K. Kakurai, *J. Phys. Soc. Jpn.* **72**, 1729 (2003).
31. A.A. Taskin, A.N. Lavrov, and Y. Ando, *Phys. Rev. Lett.* **90**, 227201 (2003).
32. D.D. Khalyavin, I.O. Troyanchuk, N.V. Kasper, Q. Huang, J.W. Lynn, and H. Szymczak, *J. Mater. Res.* **17**, 838 (2002).
33. M. Soda, Y. Yasui, M. Ito, S. Iikubo, M. Sato, and K. Kakurai, *J. Phys. Soc. Jpn.* **73**, 2857 (2004).
34. M. Soda, Y. Yasui, Y. Kobayashi, T. Fujita, M. Sato, and K. Kakurai, *J. Phys. Soc. Jpn.* **75**, 104708 (2006).
35. J. Padilla-Pantoja, C. Frontera, O. Castaño, and J.L. García-Muñoz, *Phys. Rev.* **B81**, 132405 (2010).
36. M. Kopcewicz, D.D. Khalyavin, I.O. Troyanchuk, H. Szymczak, R. Szymczak, D.J. Logvinovich, and E.N. Naumovich, *J. Appl. Phys.* **93**, 479 (2003).
37. A.A. Belik, S. Iikubo, K. Kodama, N. Igawa, S. Shamoto, S. Niitaka, M. Azuma, Y. Shimakawa, M. Takano, F. Izumi, and E. Takayama-Muromachi, *Chem. Mater.* **18**, 798 (2006).
38. J. Rodriguez, J.M. Gonzalez-Calbet, J.C. Grenier, J. Pannetier, and M. Anne, *Solid State Commun.* **62**, 231 (1987).
39. H. Kubo, K. Zenmyo, M. Itoh, N. Nakayama, T. Mizota, and Y. Ueda, *J. Magn. Magn. Mater.* **272–276**, 581 (2004).
40. L.M. Sandratskii, *Adv. Phys.* **47**, 91 (1998).
41. R.L. Withers, M. James, and D.J. Goossens, *J. Solid State Chem.* **174**, 198 (2003).

42. S.Ya. Istomin, J. Grins, G. Svensson, O.A. Drozhzhin, V.L. Kozhevnikov, E.V. Antipov, and J.P. Attfield, *Chem. Mater.* **15**, 4012 (2003).
43. S.Ya. Istomin, O.A. Drozhzhin, G. Svensson, and E.V. Antipov, *Solid State Sci.* **6**, 539 (2004).
44. D.J. Goossens, K.F. Wilson, M. James, A.J. Studer, and X.L. Wang, *Phys. Rev.* **B69**, 134411 (2004).
45. S. Ishiwata, W. Kobayashi, I. Terasaki, K. Kato, and M. Takata, *Phys. Rev.* **B75**, 220406(R) (2007).
46. S. Fukushima, T. Sato, D. Akahoshi, and H. Kuwahara, *J. Phys. Soc. Jpn.* **78**, 064706 (2009).
47. A. Baszczuk, S. Kolesnik, B. Dabrowski, O. Chmaissem, and J. Mais, *Phys. Rev.* **B76**, 134407 (2007).
48. I.O. Troyanchuk, D.V. Karpinsky, A.P. Sazonov, V. Sikolenko, V. Efimov, and A. Senyshyn, *J. Mater. Sci.* **44**, 5900 (2009).
49. I.O. Troyanchuk, D.V. Karpinsky, V.M. Dobryanskii, A.N. Chobot, G.M. Chobot, and A.P. Sazonov, *J. Exp. Theor. Phys.* **108**, 428 (2009).
50. S. Kimura, Y. Maeda, T. Kashiwagi, H. Yamaguchi, M. Hagiwara, S. Yoshida, I. Terasaki, and K. Kindo, *Phys. Rev.* **B78**, 180403(R) (2008).
51. D.V. Sheptyakov, V.Yu. Pomjakushin, O.A. Drozhzhin, S.Ya. Istomin, E.V. Antipov, I.A. Bobrikov, and A.M. Balagurov, *Phys. Rev.* **B80**, 024409 (2009).
52. D.D. Khalyavin, L.C. Chapon, E. Suard, J.E. Parker, S.P. Thompson, A.A. Yaremchenko, and V.V. Kharton, *Phys. Rev.* **B83**, 140403(R) (2011).
53. I.O. Troyanchuk, D.V. Karpinsky, and F. Yokaichiya, *JETP Lett.* **87**, 541 (2008).